《報文》 HWAHAK KONGHAK Vol. 19, NO. 3, June 1981, pp. 187–198
(Journal of the Korean Institute of Chemical Engineers)

流變工程內 非뉴톤性 流體의 移動現象에 관한 模寫硏究*

——칼렌더工程內 Bingham 流體移動——

李炳建·李載旭**·李基俊
서울大學校 工科大學 化學工學科

(접수 1981. 5. 16)

A Computer Simulation of Non-Newtonian Fluid Flow in Rheological Processes

——Bingham Fluid Flow in a Calendering Process——

Byung-Geon Rhee, Jae Wook Lee, and Ki Jun Lee**
Department of Chemical Engineering,
Seoul National University, Seoul 151, Korea

(Received May 16, 1981)

要 約

高分子物質 加工工程의 하나인 두回轉원통 사이를 흐르는 非壓縮性 粘性流의 流動現象을 Bingham 플라스틱 流體모델을 대상물질로 하여 解析하였다. 速度分布, 壓力分布等을 理論的으로 관찰하였고 또한 필름製品의 生成두께와 칼렌더의 半徑比, 回轉速度, nip distance 및 流體의 物性等의 變化에 따른 流量과 所要動力 등의 변화를 조사하였다.

半徑比를 증가시킴에 따라서 壓力은 단조 증가하는바, 이러한 증가현상은 nip distance가 작을 수록 더욱 현저하게 나타났다. 한편 nip distance가 0.01 cm인 경우 速度分布에 영향을미치는 半徑의 극한치는 0.6 cm이었으며, 이때 입구에서의 입사각은 8.6~9.0°의 범위에 있음이 밝혀졌다. 生成되는 필름의 두께는 Power-law 모델의 flow behavior index가 감소할수록 증가하고, 단위유량당의 소요동력은 nip distance가 감소할수록 증가함이 해석적으로 조사되었다.

* 産學財團 지원 연구 과제
** Present address : Department of Chemical Engineering, Sogang University, Seoul

Abstract

Non-Newtonian fluid flow between a pair of rotating cylinders with unequal size rolls and equal speed of rolls is studied theoretically for the Bingham plastic fluid model at the isothermal condition, using the bipolar cylindrical coordinates in which the boundary conditions can be prescribed exactly. A theoretical analysis of the velocity, pressure and shear stress distribution is given by solving the continuity equation and equations of motion applying the lubrication approximation.

The pressure increases monotonically with the increase of the roll radius ratio and the film thickness increases with the decrease of the flow behavior index for a constant entrance coordinate. Meanwhile, the velocity profile varies with the roll radius for the nip distance of 0.01 cm in the case that the roll radius is less than 0.6 cm. The limiting roll size is 0.6 cm and the incidence angle at the entrance point is about 8.6~9.0 degree. The power consumption per unit volumetric flow rate increases with increasing the roll speed and the roll diameter, and with decreasing the nip distance.

1. Introd ction

Calendering is a continuous operation for the production of thermoplastic sheet or film of uniform thickness. This is accomplished by a pair of heated driven rollers of equal or unequal diameters. Industrial calenders consist usually of 3-6 rotating rollers in a Z or L arrangement. The basic forming operation is completed by the calender itself and normally followed by additional treatment of the plastic film produced. The flow behavior of thin liquid films during passage through a roll nip is an important determinant of their lubricating qualities in the nip and of the characteristics of the film which emerges.

The first theoretical analysis of calendering was carried out by Ardichvili[1] in 1938 on the basis of the Reynolds lubrication theory of Newtonian hydrodynamics. In his analysis, which is restricted to a Newtonian fluid, Ardichvili assumed that the calendered fluid left off at the nip and that the final thickness(i.e. spread height) was therefore equal to the nip width. Thus, in his assumed system, pressure dropped to zero at the nip.

The hydrodynamic theory of calendering as it stands today was initially developed by Gaskell[2] and is basically similar to that of Ardichvili. His solutions for velocity and pressure distributions between two rollers and for the roll separating force are more elaborate, and extended to the calendering of Bingham plastics. Gaskell asserted that in order to analyze the calendering process correctly, it should be assumed that fluid left off at a certain distance past the nip and that pressure dropped to atmospheric at the "left off" point. The point of maximum pressure is obviously located upstream of the nip.

Later, McKelvey[3] treated the problem of calendering power-law fluids and Chong[4] derived a general equation for the true shear

rate encountered in non-Newtonian fluids. Based on several constitutive equations(a power law fluid, a three constant Oldroyd fluid and a modified second-order Rivlin-Ericksen fluid), he analyzed calendering from the hydrodynamic point of view. Brazinsky et. al.[5] analyzed the relationship between spread height and upstream reservoir thickness, with power law coefficient as parameter. Alston and Astill[6] predicted the one-dimensional behavior of a hyperbolic tangent fluid model flowing between calendering rollers. Accurate power consumption calculations have been carried out by Ehrmann and Vlachopoulos.[7] The asymmetrical problem(i.e., flow between rolls rotating at different speeds or rolls of different diameters) had not drawn much attention despite its practical importance. Recently, however, Takserman-Krozer et.al.[8] treated the asymmetrical problem analytically by using the bipolar cylindrical coordinates.

In the present study, non-Newtonian fluid flow between a pair of rotating cylinders with unequal size rolls and/or equal speed of the rolls is studied theoretically for the Bingham plastic fluid model at the isothermal conditions. The finite difference method[9,10] is employed using the bipolar cylindrical coordinates[11] which exactly satisfies the prescribed boundary conditions on the surface of the rolls and estabilshes an orthogonal network with uniform mesh size for each of the variables. A theoretical analysis of the velocity, pressure and shear stress distribution in the flow field is given by solving the continuity equation and equations of motion applying the lubrication approximation.

2. Mathematical Model and Governing Equations

An incompressible Bingham fluid flow between geometrically asymmetric calender rolls is studied at the isothermal condition. The radii of the rolls are R_1 and R_2, their rotating speed is U_1 and their separating distance at the nip is H. Geometrical parameters are illustrated in *Fig 1*. The bicylindrical geometry of the boundary conditions can most easily be accommodated by using the bipolar cylindrical coordinates ξ and η, where

$$\xi = \angle A_1 P A_2 \qquad (2\pi \geqslant \xi \geqslant 0) \tag{1}$$

$$\eta = \left| \ln \frac{r_2}{r_1} \right| \qquad (-\infty < \eta < \infty) \tag{2}$$

The ξ and η are dimensionless quantities and form a set of two dimensional orthogonal curvilinear coordinates. The metric tensor of the bipolar coordinates has two equal components

$$g_{11} = g_{22} = h^2 \tag{3}$$

where

$$h = \frac{a}{\cosh \eta - \cos \xi} \tag{4}$$

For sufficiently small value of η ($H \ll R_1, R_2$), it is approximately given by function of ξ only such that

$$h = \frac{a}{1 - \cos \xi} \tag{5}$$

The conventional assumptions are made such that the axial length L of the cylinders, the length of the curved channel formed by the rolls and the radii of the rolls are very large compared with the separation H at the nip. So the flow can be taken to be two dimensional. A highly viscous fluid is introduced to flow in creeping motion between calendering rolls so that inertia forces and body forces are negligibly small in compari-

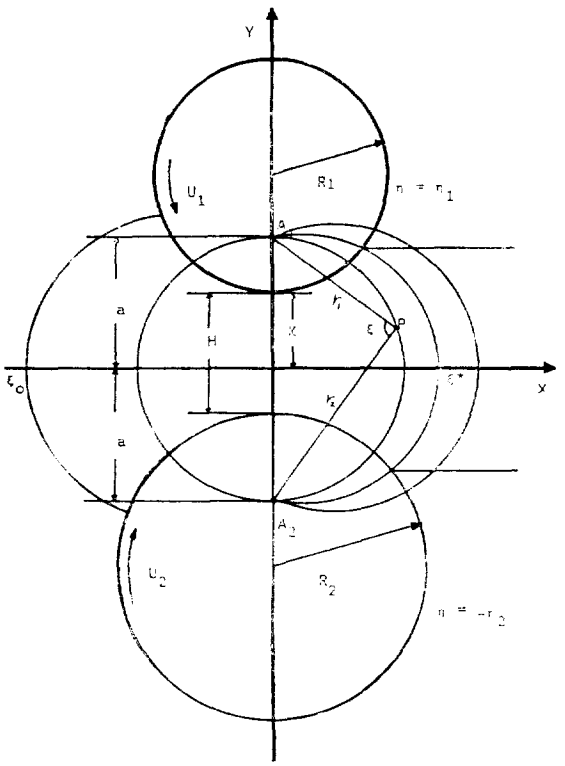

Fig. 1. Calender Rolls Geometry in the Bipolar Cylindrical Coordinates

son with the viscous forces. Furthermore, it is assumed that the rollers are completely rigid, i.e., the pressure built up in the fluid does not distort the calendering cylinders. By the simplifying assumptions and using the lubrication approximation, the equation of continuity and the equations of motion become as follows.

Equation of continuity:

$$\frac{\partial}{\partial\xi}(hU)+\frac{\partial}{\partial\eta}(hV)=0 \tag{6}$$

Equations of motion:

$$\frac{\partial P}{\partial\xi}=\frac{\partial\tau_{\xi\eta}}{\partial\eta} \tag{7}$$

$$\frac{\partial P}{\partial\eta}=0, \tag{8}$$

where U and V are the velocity components along the curvilinear coordinates ξ and η.

The constitutive equation is now given for the Bingham fluid by

$$\tau_{\xi\eta}=-\left\{m\left|\frac{\partial}{\partial\eta}\left(\frac{U}{h}\right)\right|^{n-1}\right\}\frac{\partial}{\partial\eta}\left(\frac{U}{h}\right)\pm\tau_0 \quad : |\tau_{\xi\eta}|>\tau_0 \tag{9-a}$$

$$\frac{\partial}{\partial\eta}\left(\frac{U}{h}\right)=0 \quad : |\tau_{\xi\eta}|<\tau_0 \tag{9-b}$$

where m and n are the flow consistency index and the flow behavior index of Bingham plastic fluid.

The boundary conditions for the asymmetric calendering become, by the conditions of no slip and isothermal solid walls,

$U=U_1$ at the wall of the rolls (10)

$V=0$ at the wall of the rolls (11)

To find the relationship between the entrance coordinate ξ_0 and the exit coordinate ξ^*, it is assumed that when the material enters and leaves the deformation zone the pressure will be equal to zero and its derivative at the exit coordinate equals to zero:

$$P=0 \qquad at\ \xi=\xi_0 \tag{12}$$

$$P=0,\ \frac{\partial P}{\partial\xi}=0 \qquad at\ \xi=\xi^* \tag{13}$$

To find the locus of yield stress τ_0, integration of eq. (7) leads to

$$\int_0^{\tau_0} d\tau_{\xi\eta}=\int_{\frac{\eta'-\eta_2'}{2}}^{\eta'}\frac{\partial P}{\partial\xi}\,d\eta \tag{14}$$

$$\left(\frac{\eta'+\eta_2'}{2}\right)_i=\frac{\tau_0}{(\partial P/\partial\xi)_i} \tag{15}$$

Here η' and η_2' are the loci of the points where the shear stress equals to the yield stress τ_0 in the upper and lower parts, respectively.

3. Theoretical Analysis

The velocity distribution of the Bingham plastic fluid in the deformation area of the calender is divided into three parts:

i) $\eta'<\eta\leq\eta_1$, ii) $-\eta_2\leq\eta<-\eta_2'$ and

iii) $-\eta_2'\leq\eta\leq\eta_1'$

In part i) and ii) fluid flows somewhat like a Newtonian fluid but in part iii) the velocity gradient is zero so it becomes plug flow. The velocity distribution is obtained by integrating the equation of motion with respect to η using the boundary conditions:

$$i)\ U = U_a = U_1 - h\left(\frac{1}{m}\right)^{1/n}\left(\frac{\partial P}{\partial \xi}\right)^{1/n} \cdot \frac{n}{n+1}\{(\eta_1 - \eta_1')^{(n+1)/n} - (\eta - \mu_1')^{(n+1)/n}\} \tag{16}$$

$$ii)\ U = U_b = U_1 - h\left(\frac{1}{m}\right)^{1/n}\left(\frac{\partial P}{\partial \xi}\right)^{1/n} \cdot \frac{n}{n+1}\{(\eta_2' - \eta_2)^{(n+1)/n} - (\eta + \eta_2')^{(n+1)/n}\} \tag{17}$$

$$iii)\ U = U_c = U_1 - h\left(\frac{1}{m}\right)^{1/n}\left(\frac{\partial P}{\partial \xi}\right)^{1/n} \cdot \frac{n}{n+1}(\eta - \eta_1')^{(n+1)/n} \tag{18}$$

Here $\frac{\partial P}{\partial \xi}$, η_1' and η_2' are the pressure gradient and the loci of the yield stress, which are defined as function of ξ.

Integration of the equation of continuity with respect to η using boundary condition (11) from $-\eta_2$ to η_1 gives

$$\int_{-\eta_2}^{\eta_1} \frac{\partial}{\partial \xi}(hU)\,d\eta = 0 \tag{19}$$

so that the volumetric flow rate through the rolls per unit width at steady state is written by the integral form

$$Q = \int_{-\eta_2}^{\eta_1} hU\,d\eta = \int_{\eta_1'}^{\eta'} hU_a\,d\eta + \int_{-\eta_2}^{-\eta_2'} hU_b\,d\eta + \int_{-\eta_2'}^{\eta_1'} hU_c\,d\eta \tag{20}$$

The volumetric flow rate is constant for each cross section and independent of the position ξ.

From the equations (16), (17), (18) and (20) the pressure gradient is defined as follows:

$$\left(\frac{\partial P}{\partial \xi}\right)^{1/n} = (2n+1)m^{1/n}(h-h^*)U_1 \cdot (\eta_1+\eta_2)/nh^2\left[\{(\eta_1 - \eta_1')^{(2n+1)/n} - (\eta_2' - \eta_2)^{(2n+1)/n} + \frac{2n+1}{2(n+1)}(\eta_1' + \eta_2')\right\}\{(\eta_1 - \eta_1')^{(n+1)/n} + (\eta_2 - \eta_2)^{(n+1)/n}\}\right] \tag{21}$$

The nonlinear algebraic equations with respect to the pressure gradient and two variables (η_1', η_2') which are the functions of the independent variable ξ only, may be solved by using the Newton-Raphson iteration scheme. The function f_1, f_2 and f_3 are defined from the equations (15), (18) and (21) as follows:

$$f_1 = (\eta_1 - \eta_1')^{(n+1)/n} - (\eta_2' - \eta_2)^{(n+1)/n} \tag{22}$$

$$f_2 = (2n+1)m^{1/n}(h-h^*)U_1(\eta_1+\eta_2)/\left[\{(\eta_1 - \eta_1')^{(2n+1)/n} - (\eta_2' - \eta_2)^{(2n+1)/n} + \frac{2n+1}{2(n+1)}(\eta_1' + \eta_2')\{(\eta_1 - \eta_1')^{(n+1)/n} + (\eta_2' - \eta_2)^{(n+1)/n}\}\right] nh^2 - \left(\frac{\partial P}{\partial \xi}\right)^{1/n} \tag{23}$$

$$f_3 = \frac{\tau_0}{(\partial P/\partial \xi)_i} - \left(\frac{\eta_1' + \eta_2'}{2}\right)_i \tag{24}$$

Considerable interest centers around the shape of the pressure profile through the nip. The pressure field between the rolls is obtained by integratng the pressure gradient of the each cross section.

$$P = \int_{\xi}^{\xi^*} \frac{\partial P}{\partial \xi}\,d\xi \tag{25}$$

There is another location significant for the pressure distribution calculation and called the entrance coordinate(ξ_0) at which pressure becomes zero.

$$\int_{\xi_0}^{\xi^*} \frac{\partial P}{\partial \xi}\,d\xi = 0 \tag{26}$$

The relationship between the entrance and the exit coordinate is deduced from equation (26).

The power dissipated in the flow field between the rotating rolls is generally given

by the following expression:

$$W = \int_{\xi 0}^{\xi^*} \int_{-\eta_2}^{\eta_1} \tau \dot{\gamma}_{\eta\xi} \, d\eta \, d\xi \tag{27}$$

The power requirement per unit volumetric flow rate can be described by E = W/Q which is an important characteristics of the calendering process, as it expresses the specific energy requirement of a process.

The forces exerted by the fluid flowing between the rolls tend to separate them. This roll separating force per unit width is given by

$$F = \int_{\xi 0}^{\xi^*} hP \, d\xi \tag{28}$$

4. Results and Discussion

The velocity, pressure and shear stress distribution in the flow field are obtained numerically by using the Newton-Raphson method.

A schematic diagram of the velocity profiles is shown in *Fig 2*. The broken lines represent the locus of yield stress (η_1', $-\eta_2'$). In the region where $\eta_1' < \eta \leq \eta_1$ and $-\eta_2 \leq \eta < -\eta_2'$ the velocity varies, but in the region $-\eta_2' \leq \eta \leq \eta_1'$, the velocity is constant because the shear stress is smaller than the yield stress. In the region between $\xi = \xi^*$ and $\xi = 2\pi - \xi^*$, the volocity profile is convex because the pressure gradient is negative. In the region where $\xi > 2\pi - \xi^*$, the pressure gradient becomes positive and the forward fluid motion is retarded, causing the velocity profile to be concave. As ξ increases, a point is eventually reached where the fluid velocity at the mid-plane becomes zero. This is called stagnation point(ξ_s). In the region where $\xi > \xi_s$, the velocity component changes sign as η varies for a given value of ξ. This suggests that near the mid-plane fluid moves away from the nip of the rolls because the velocity components are negative but that near the roll surface the velocity components are positive and the fluid moves toward the nip. The net result is a partial circulation of the fluid in the region $\xi > \xi_s$. This circulation should form closed cellular vortices in

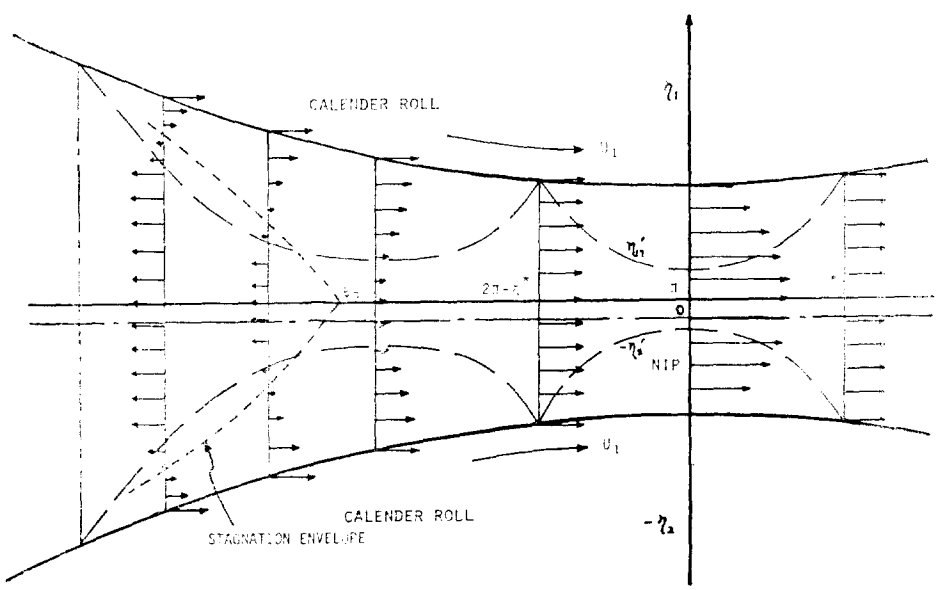

Fig. 2. Schematic Diagram of Velocity Distribution and Stagnation Envelope

the rotating bank. Actually, there are infinite numers of stagnation points that form an envelope. This is called the "stagnation envelope". The locus of the stagnation envelope is represented as dotted line in *Fig. 2*

Fig. 3 shows the velocity distributions at the nip point, where the velocity profile is convex and increases with decreasing power law index near the roll surface but near the center the profile decreases. *Fig. 4* shows the relationship between the symmetric and asymmetric calender. For symmetric case, η varies from -0.0245 to 0.0245 but η varies from -0.0163 to 0.0245 for asymmetric case. It is noted that the center of symmetry is a half of the nip distance, i.e., there is no effect of geometrical asymmetry. This is caused by the order of magnitude between the roll radius and the nip distance. For a constant nip distance, the roll size which gives an effect on velocity profile is found in *Table 1*. The variation of roll radius does not affect the velocity profile significantly as long as the roll radius is very large compared with the nip distance. However, the velocity profile varies with the roll radius for the nip distance of 0.01 cm in the case that the roll radius is less than 0.6 cm. The limiting roll size is 0.6 cm and the incidence

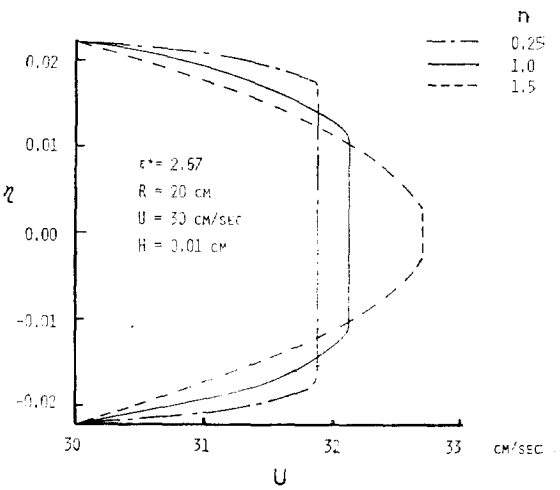

Fig. 3. Velocity Distribution at the Nip Point

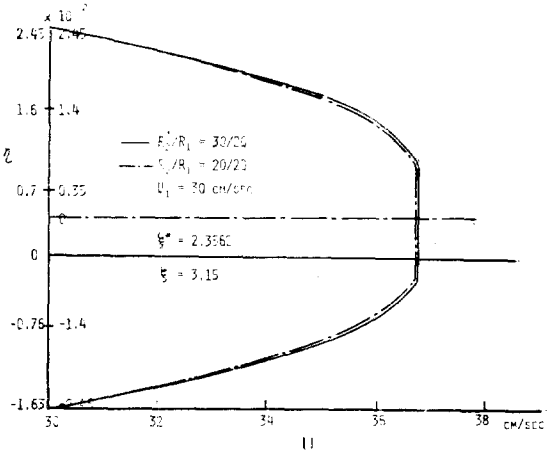

Fig. 4. Comparison of Velocity Distributions between Symmetric and Asymmetric Cases

Table 1. The Relationship between the roll size and the incidence angle

R	η	ξ	$\tan\theta$	θ	Velocity at $\xi=\pi$	
cm	—	—	—	deg.	near wall	near center
0.06	0.405	5.256	0.487	25.95	34.246	36.842
0.1	0.315	〃	0.374	20.48	34.244	36.844
0.2	0.223	〃	0.263	14.71	34.243	36.846
0.4	0.158	〃	0.185	10.50	34.242	36.847
0.5	0.141	〃	0.165	9.41	34.242	36.848
0.6	0.129	〃	0.151	8.60	34.241	36.848
1.0	0.100	〃	0.117	6.70	〃	〃
10.0	0.032	〃	0.037	2.12	〃	〃

angle at the entrance point is about 8.6—9.0 degree.

Fig. 5 and *6* represent the pressure profiles for various flow behavior index and various nip distance respectively. The pressure significantly decreased and the entrance coordinate slightly increased with decreasing flow behavior index and increasing nip distance. The maximum pressure is very sensitive to the varition of the exit coordinate. A decrease in the exit coordinate brings about both a broadening the pressure profile as well as an increase in the maximum value of the pressure. This is demonstrated in *Fig. 7*. The pressure profiles for various roll diameter are illustrated in *Fig. 8*. It shows that the pressure increased with increasing roll diameter at constant nip distance. *Fig. 9* shows that the radius ratio affects the pressure profile. It is noted that at constant (R_1), the pressure is a monotonically increasing function of $\alpha(R_2/R_1)$. With the increase of α, the pressure increases. This increment is more significant for small values of H(see curve 1 in *Fig. 9*). With increasing H the curve $P(\alpha)$ is flattened(see curves 2 and 3 in *Fig. 9*). *Fig. 10* shows the power consumption per unit volumetric flow rate increases wtih decreasing the nip distance.

5. Conclusion

A geometrically asymmetric calendering process is analyzed theoretically by using Bingham plastic fluid model and several significant conclusionsions were drawn as follows:

1) The pressure increases monotonically with the increase of the roll radius ratio. The

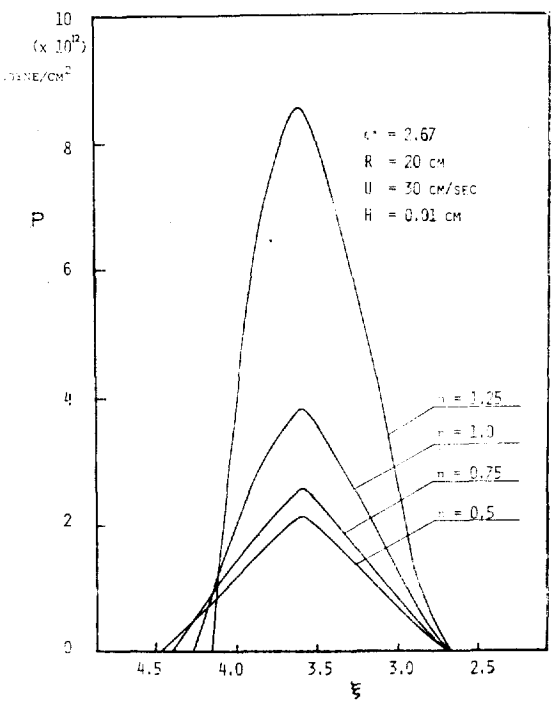

Fig. 5. Pressure Profiles of various Flow Behavior Indices

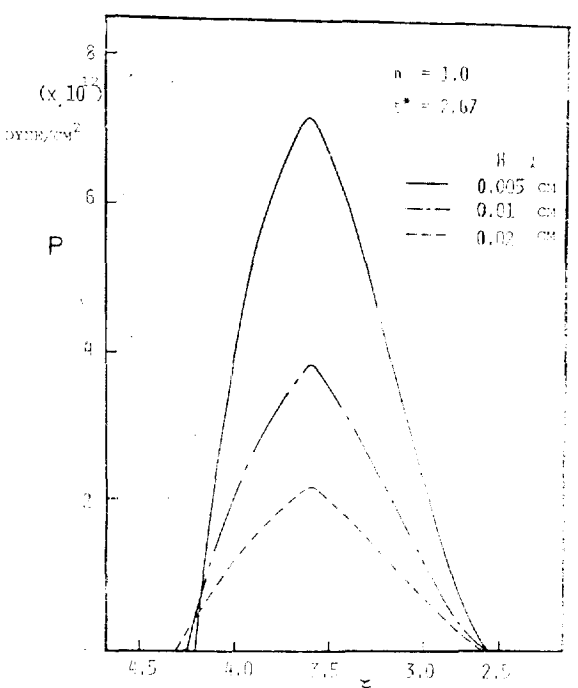

Fig. 6. Pressure Profiles for various Geometry of the Calender

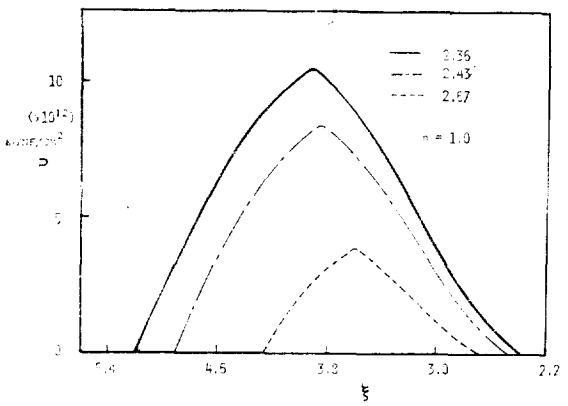

Fig. 7. Pressure Profiles for various Film Thickness

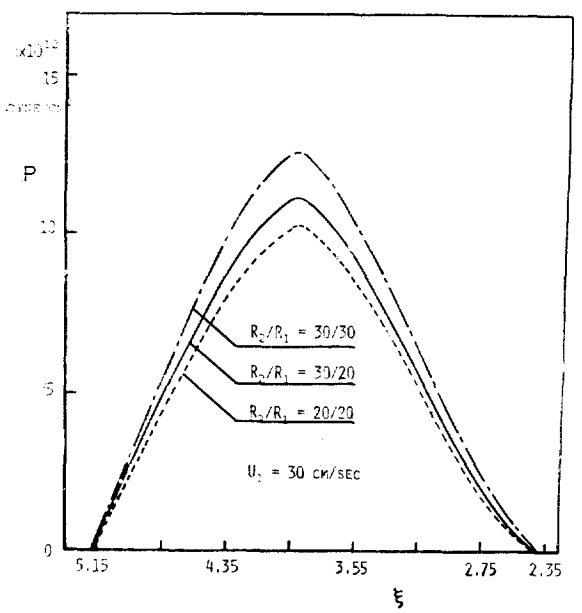

Fig. 8. Pressure Profiles for various Roll Diameter

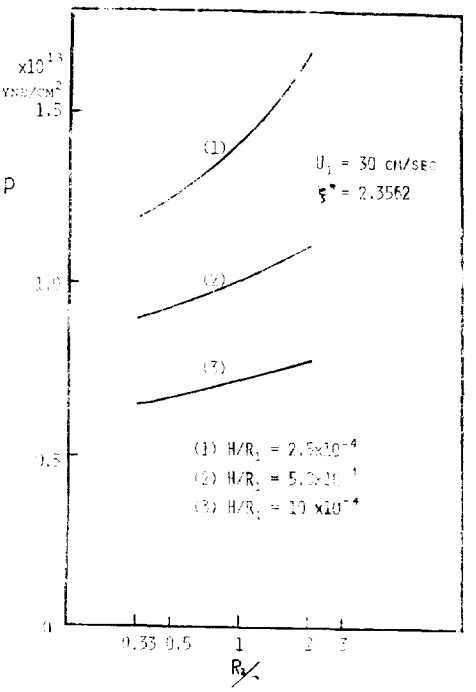

Fig. 9. Pressure Profiles for various Radius Ratio

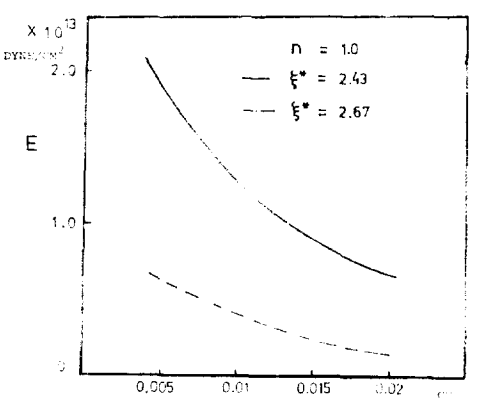

Fig. 10. Nip Distance vs. Power Consumption Change per Unit Volumetric Flow Rate

increase is more significant for small values of the roll separation at the nip.

2) The film thickness increases with the decrease of the flow behavior index (n) for a constant entrance coordinate.

3) The variation of roll radius does not affect the velocity profile significantly as long as the roll radius is very large compared with the nip distance. However, the velocity profile varies with the roll radius for the nip distance of 0.01 cm in the case that the roll radius is less than

0.6 cm. The limiting roll size is 0.6 cm and the incidence angle at the entrance point is about 8.6-9.0 degree.

4) The power consumption per unit volumetric flow rate increases with increasing roll diameter and decreasing the nip distance.

Acknowledgment

The authors gratefully acknowledge the Korea Traders Scholarship Foundation for financial support of this research. Parts of this work were presented at the 1980 annual Autumn meeting of the Korean Institute of Chemical Engineers.

Nomenclature

a	half the distance between the poles(cm)
A_1, A_2	pole points
E	power consumption per unit volumetric flow rate(dyne/cm²)
F	roll separating force per unit width(dyne)
f_1, f_2, f_3	functions of eq. (22)-(24)
g_{ij}	components of the metric tensor
h	variable defined by eq. (5)(cm)
h^*	h at $\xi = \xi^*$(cm)
H	roll separation at the nip(cm)
L	axial length of the cylinders(cm)
m	flow consistency index(g/cm sec)
n	flow behavior index
P	pressure(dyne/cm²)
P_{max}	maximum pressure(dyne/cm²)
Q	volumetric flow rate per unit width (cm³/sec)
Q^*	Q at $\xi = \xi^*$(cm³/sec)
r_1, r_2	distance of a point from the poles of the bipolar coordinates(cm)
R_1, R_2	radius of upper and lower calendering roll(cm)
U_1	rotating surface velocity of the roll (cm/sec)
U, V	velocity components into the ξ, η direction(cm/sec)
W	dissipated power(dyne cm/sec)
X, Y	cartesian coordinates

Greek Letters

α	radius ratio($\alpha = R_2/R_1$)
β	dimensionless gap between the rolls ($\beta = H/R_1$)
$\dot{\gamma}_{ij}$	components of the rate of strain tensor
ξ, η	bipolar cylindrical coordinates
η_1, η_2	values of η at the wall of the rolls
η_1', η_2'	locus of the yield stress
ξ_0	entrance coordinate
ξ^*	exit coordinate
τ	shear stress(dyne/cm²)
τ_{ij}	components of the stress tensor
τ_0	yield stress(dyne/cm²)
τ_{w1}, τ_{w2}	shear stress at the wall of the rolls (dyne/cm²)

Bibliography

1. G. Ardichvili, "An Attempt at a Rational Determination of the Cambering of Calender Rolls," Kautschuk, **14** (1938), 23.
2. R.E. Gaskell, "The Calendering of Plastic Materials," J. Appl. Mech., **17** (1950), 334.
3. J.M. McKelvey, "Polymer Processing," Wiley, New York, 1962.
4. J.S. Chong, "Calendering Thermoplastic Materials," J. Appl. Polymer Sci., **12** (1968), 191.
5. I. Brazinsky, H.F. Cosway, C.F. Valle, Jr., R. Clark Jones and V. Story, "Film Spread Heights in the Calendering of

Newtonian and Power Law Fluids," J. Appl. Polymer Sci., **14** (1970), 2771.

6. W.W. Alston, Jr. and K.N. Astill, "An Analysis for the Calendering of Non-Newtonian Fluids," J. Appl. Polymer Sci., **17** (1973), 3157.
7. G. Ehrmann and J. Vlachopoulos," Determination of Power Consumption in Calendering," Rheol. Acta, **14** (1975), 761.
8. R. Takserman-Krozer, G. Schenkel and G. Ehrmann, "Fluid Flow between Rotating Cylinders," Rheol. Acta, **14** (1975), 1066.
9. B. Carnahan, H.A. Luther and J.O. Wilkes, "Applied Numerical Method," Wiley, New York, 1969.
10. P.J. Roache, "Computational Fluid Dynamics," Hermosa Publishers, Albuquerque, 1976.
11. J. Happel and H. Brenner, "Low Reynolds Number Hydrodynamics," Prentice-Hall, Englewood, N.J., 1965.
12. R.B. Bird, W.E. Stewart and E.N. Lightfoot, "Transport Phenomena," Wiley, New York, 1960.
13. S. Middleman, "Fundamentals of Polymer Processing," McGraw-Hill, New York, 1977.
14. R.B. Bird, R.C. Armstrong, O. Hassager and C.F. Curtiss, "Dynamics of Polymeric Liquids," Vol. 1: Fluid Mechanics, Vol. 2. Kinetic Theory, Wiley, New York, 1977.